https://doi.org/10.48048/tis.2024.8308

Effect of Dy^{3+} Concentrations on the Structural and Optical Properties of $SrAl_2O_4:Eu^{2+}$, Dy^{3+} NPs

Victor Kadenge[1,*], Sharon Kiprotich[2], Millien Kawira[1] and Ali Wako[1]

[1]*Department of Physical Sciences, University of Embu, Embu, Kenya*
[2]*Department of Physical and Biological Sciences, Muranga University of Technology, Muranga, Kenya*

([*]Correspondence author's Email: 1359@student.embuni.ac.ke)

Received: 13 April 2024, Revised: 15 May 2024, Accepted: 30 May 2024, Published: 20 August 2024

Abstract

Recently, there has been extensive research on the synthesis of luminescent particles, as these materials show great potential for various industrial uses. Multiple matrices have been formulated, with the $SrAl_2O_4:Eu^{2+}$, Dy^{3+} matrix being the most extensively studied due to its superior optical and structural properties. In this work, the objective of synthesizing $SrAl_2O_4:Eu^{2+}$, Dy^{3+} particles were achieved by using a combustion approach. By optimizing the synthesis process and studying the impact of Dy^{3+}concentrations on the structural and optical features, it has proven feasible to regulate the reaction and attain exceptional optical characteristics. The importance of this investigation is in assessing the practical feasibility of using such a material. This study examines a phosphor composed of strontium aluminate ($SrAl_2O_4$) that is activated using various amounts of Dy^{3+}(ranging from 0.1 to 0.8 mol %). The study's findings of XRD showed that the $SrAl_2O_4:Eu^{2+}$, Dy^{3+}samples had a monoclinic phase of space group P_{21}. Increase in the dopant concentration, the size of the crystallites in $SrAl_2O_4:Eu^{2+}$, Dy^{3+} samples decreased, as determined by Scherer's formula and the Williamson-Hall plot. The bandgap energy of doped $SrAl_2O_4:Eu^{2+}$, Dy^{3+} nanoparticles was estimated using a Tauc plot based on data collected from an ultraviolet visible spectrophotometer. The results showed that the bandgap energy decreased from 6.5 to 5.5 eV as the level Dy^{3+}rose from 0.1 to 0.8 mol %. FT-IR spectroscopy revealed a prominent vibrational stretching at 570 cm^{-1}, which is likely due to the Al-O bond, and another stretching at 1049 cm^{-1}, related to the Sr-O bonds of $SrAl_2O_4:Eu^{2+}$, Dy^{3+} NPs.

Keywords: Long afterglow, Strontium aluminate, Lattice strain, Dislocation density, Energy bandgap, Crystallite Size, Co-dopant.

Introduction

Long-lasting phosphors (LLPs) have been a focal point for study for a long time due to their essential role in our day-to-day activities [1]. Luminescent nanomaterials have been extensively utilized in various fields, including decorative goods, luminous timepieces, evacuation corridor lighting, escape symbols, roadway markings, biosensing, military usage, and in vitro imaging [2]. LLPs have significant potential for uses like textiles, solar, Vacuum fluorescent displays (VFDs), Field emission displays (FEDs**)** [3] etc. Copper-doped zinc sulfide was previously the most often used long-lasting phosphorescent material, known for its high sensitivity to high humidity and short afterglow [4]. Alkaline earth aluminate LLPs doped incorporating rare earth ions, like strontium aluminate, have been prepared for their extended phosphorescence properties and excellent quantum efficiency. Matsuzawa *et al.* [5] achieved the first

practical synthesis of $SrAl_2O_4:Eu^{2+}$, Dy^{3+}, a compound with rare earth ions commonly used for doping in alkaline earth aluminates. Some scientists have since focused on enhancing the luminous intensity and longevity of the durable strontium aluminate-based phosphor [6,7]. The process of afterglow still needs to be completed. The new study focuses on modifying the brilliant features of phosphors. The key characteristics of the nanophosphor in monitors and luminescence, like light intensity and colour emission are influenced by factors like morphology, and surface qualities, imperfections and co-activator concentrations [8,9]. Varying the concentration of dysprosium can modify the related structure, physical, mechanical, electronic, and mobility of ceramics by depositing extreme energy in the substance [10]. When co-dopants interact with the phosphor material, it leads to electronic excitation or ionization, causing a rise in temperature along the ion beam's trajectory. The increase in temperature creates a pressure wave that spreads heat widely within the intended area, leading to decreased crystallinity of the materials [4]. When dealing with insulators or luminescent nanomaterials, co-dopants can alter the material characteristics by inducing dislocations , forming novel colour centres, and rearranging trapping or luminous centres [11,12]. Zhang *et al.* [13] documented an increase in afterglow in $BaAl_2O_4:Eu^{3+}$ when co-doped with Nd^{3+}. There are scanty publications regarding the alteration of Dy^{3+}concentrationin strontium aluminate nanoparticles.

The combustion approach shows potential as a viable method for producing various types NPs. This method is very adaptable, efficient, that it operates at low temperatures. It enables homogeneous doping in just one procedure and does not require a reduced atmosphere for powder preparation. Particles that are produced through conventional combustion procedures have a nanoscale size limit. These particles tend to agglomerate, but they are less dense and more sintered compared to particles produced through other techniques.

In this study, we propose a simple approach to develop $SrAl_2O_4:Eu^{2+}$, Dy^{3+} nanostructured powders with varying concentration of Dy^{3+} ratios. Analyzing the effects of an increase in co-dopant concentrations in strontium aluminate doped with europium is valuable due to the generation and rearrangement of colour centres during synthesis, which can alter the phosphor's luminous properties [14].

Materials and methods

Solution combustion technique was used to prepare $SrAl_2O_4:Eu^{2+}$, Dy^{3+} phosphors. All starting materials were of analytical grades from Kobian scientific (Kenya). The starting chemicals $Sr(NO_3)_2$ 98.9 % , $Al(NO_3)_3{\cdot}9H_2O$ 99.9 % , $Eu(NO_3)_3{\cdot}6H_2O$ 99.9 % $Dy(NO_3)_3{\cdot}5H_2O \geq$ 98.9 % were used alongside urea $NH_2CONH_2 \geq$ 99.9 % 20 g as the fuel. The metal nitrates were weighed in $Sr(NO_3)_2$:$Al(NO_3)_3$ 1:2 mol % and $Eu(NO_3)_3$held constant at 1 mol % as $Dy(NO_3)_3$ was varied from 0.1 to 0.8 mol % were mixed then dissolved in 10 mL of deionized water while stirring on a magnetic stirrer until a transparent solution was created. A dense mixture was transferred to the crucible and placed in a preheated muffle furnace at 700 °C for 5 min. The gel-like substance was first heated, then dried, and ultimately broken down, releasing a significant amount of gasses namely carbon dioxide and nitrogen. The formed froth was cooled at around 25 °C and then finely ground using a pestle and mortar.$SrAl_2O_4:Eu^{2+}$,Dy^{3+}nanophosphors characterization was conducted using a Rigaku Miniflex XRD, with CuKα (0.15406 nm) radiation, spanning the angle range of 2θ (10°-70°), to analyse the phases present, lattice parameters, crystallite size and stress of the phosphors. The sample diffractogram was analyzed using the PCPDFWIN software for phase identification. (UV-Vis) Perkin Elmer, Lambda 950 was used to investigate the material's optical energy band gap. Fourier transform infrared spectrometer (FTIR) equipment was utilized to examine the functional group (1400 - 4000 cm^{-1}) of the as-prepared nanomaterial.

Results and discussion

Structural studies

Figure 1 shows diffraction profiles of $SrAl_2O_4:Eu^{2+}$ nanophosphors co-doped with $Dy^{3+}$with the standard data file (JCPDS No. 34-0379). The peaks of diffraction detected were characterized by their sharpness and broadened, indicating that the synthesized samples were completely nanocrystalline and polycrystalline. They were a good match alongside the standard JCPDS data file (No. 34-0379) [15,16] for the $SrAl_2O_4$monoclinic phase with space group P_{21}. However, there were no peak-linked dopant ions. This suggests that the dopant ions were spread out evenly in the host material (Sr). As the Dy^{3+} concentration was raised, no new peaks corresponding to other phases were seen. This suggests that the structure of the $SrAl_2O_4$ nanomaterial is very stable[17].

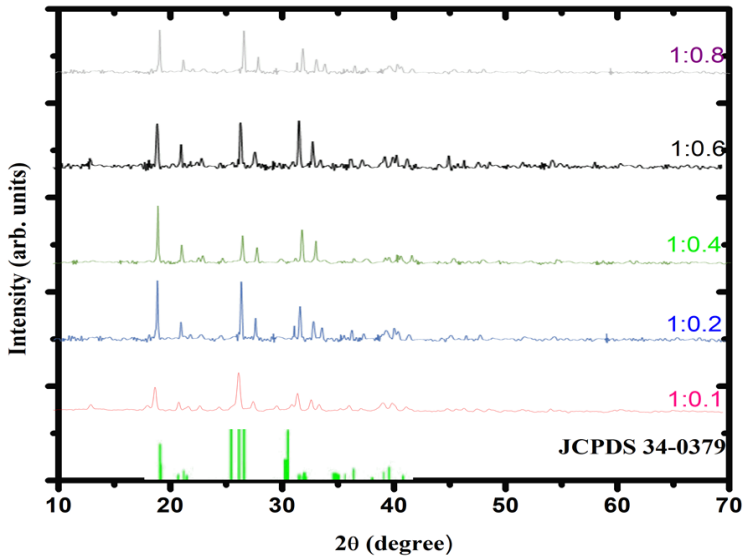

Figure 1 XRD profile of $SrAl_2O_4:Eu^{2+}$with varying concentration of Dy^{3+}.

As the Dy^{3+} content went up, the diffraction peaks got less intense, but they didn't move much in terms of where they were. It's possible that the changes in the peak intensity were caused by defects appearing as the Dy^{3+} concentration rose. It has also been seen that as the Dy^{3+} content increases, the peak broadens (FWHM) as seen in **Figure 2**. These facts show that as the quantity of the co-dopant rises, the material loses crystallinity. The well-known Debye-Scherer [18] Eq. (1) was used to determine the crystallite size D of the $SrAl_2O_4:Eu^{2+}$, Dy^{3+} phosphor.

$$D = \frac{K\lambda}{\beta cos\theta} \quad (1)$$

The crystallite sizes were estimated to be 32.23, 31.69, 30.99, 30.75, and 29.77 nm as the Dy^{3+} concentration increased. An increase in Dy^{3+}concentration leads to a broadening of XRD peaks, suggesting a reduction in the crystallite size of the $SrAl_2O_4:Eu^{2+},Dy^{3+}$ [19]. Both the lattice strain (ε) and crystallite size D were determined. This strain may have developed as a result of the existence of Dy^{3+} dopant [20] in the host matrix. The predicted strain rose as the dopant levels rose, as seen in **Table 1**. The discrepancy in crystallite size obtained from the Debye-Scherer (**Figure 2**) and Williamson-Hall(**Figure 4**) is due to that Williamson-Hall accounts for broadening produced by tensile strain factors [21]. All approaches' outcomes showed that a rise in strain as the doping concentration increased from 0.1 to 0.8 % led to a reduction in

crystal size. Various studies have revealed a consistent pattern of crystal size alteration in Dy^{3+} doped $SrAl_2O_4$ nanoparticles [5]. The decrease in $SrAl_2O_4$ crystal size is observed as the $SrAl_2O_4$ doping concentration rises, indicating that the growth was hindered by introducing Dy^{3+} ions into the Sr site [22]. This is due to the incorporation of the ions of Dy^{3+} into the host lattice., which generates additional nucleation sites, leading to increased lattice strain and slowing down crystal formation [23,24]. Due to microstructural strain and other defects, the dislocation density, δ rises with higher levels of Dy^{3+} doping in the host lattice [25] (**Figure 3**).

$$\delta = \frac{1}{D^2} \quad (2)$$

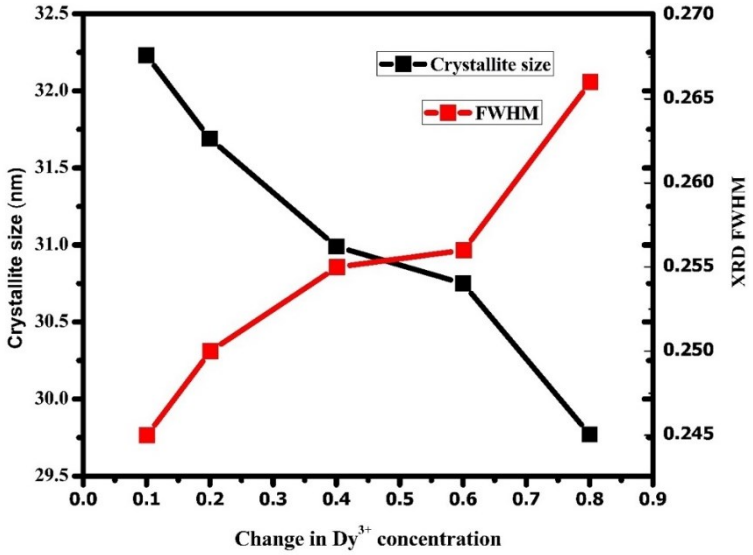

Figure 2 Crystallite size and FWHM analysis of $SrAl_2O_4:Eu^{2+},Dy^{3+}$ with changing Dy^{3+} concentration.

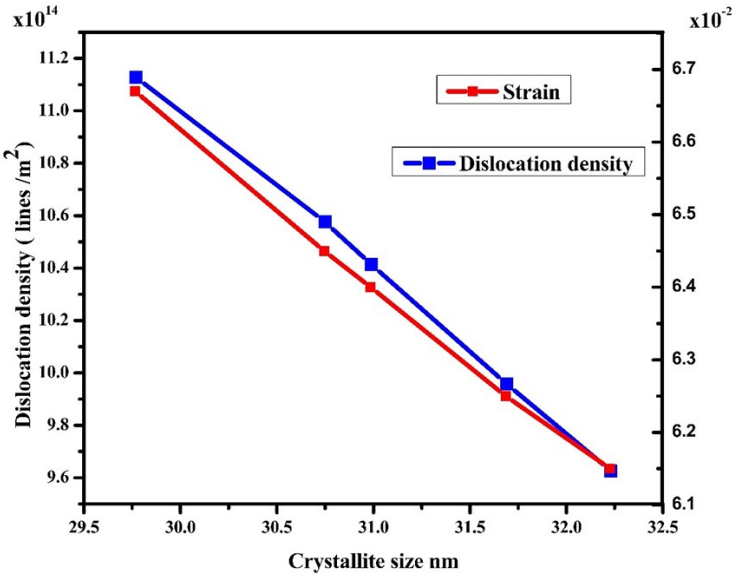

Figure 3 Relationship between dislocation density and strain as a function of crystallite size.

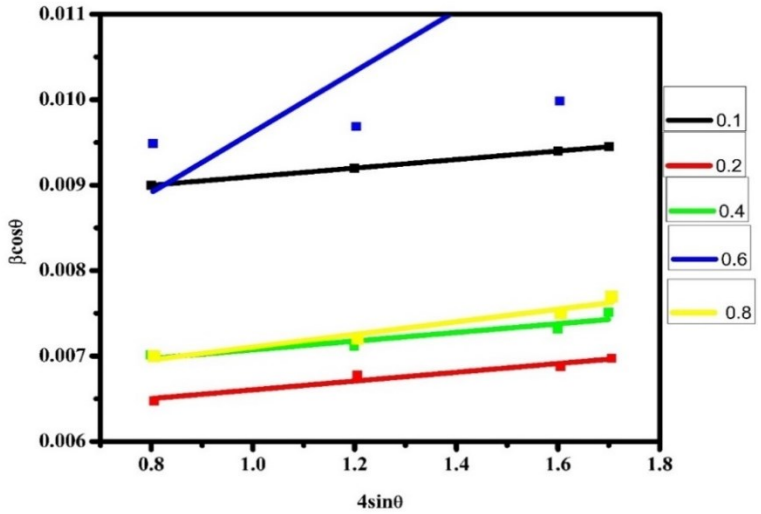

Figure 4 W-H plots ($\beta cos\theta \ against \ 4 \ sin \ \theta$)of co-doped $SrAl_2O_4:Eu^{2+}$, Dy^{3+} at different concentrations of Dy^{3+}molar ratios.

Table 1 The structural parameters and optical bandgap of co-doped strontium aluminate nanoparticles.

Doping concentration	Scherrer's method D (nm)	Dislocation density $\times 10^{14}$ lines/m^2	W-H method D (nm)	Strain	Lattice parameter	Energy Band energy eV
0.1	32.23	9.626	33.19	6.15×10^{-2}	0.84470	6.5
0.2	31.69	9.958	32.56	6.25×10^{-2}	0.84465	6.3
0.4	30.99	10.413	31.38	6.40×10^{-2}	0.84380	6.0
0.6	30.75	10.576	30.72	6.45×10^{-2}	0.84360	5.7
0.8	29.77	11.128	29.81	6.67×10^{-2}	0.8420	5.5

FTIR Analysis

Figure 5 displays the IR spectrum of the host containing ($0.1 \leq x \leq 0.8$ mol %) of Dy^{3+} used to analyze the functional compounds and vibrational frequencies in the produced NPs. The vibration seen at 570 cm^{-1} is probably attributed to the Al-O bond vibrations [7]. The absorption band at 770 cm^{-1} and the strong stretching band at 1260 cm^{-1} [7] are likely connected with the stretching of the Sr-O bonds [7]. The prominent peaks at 2882 and 2964 cm^{-1} [26,27]are probably due to the C=O bond found in carbon II oxide from the environment[28]. The spectrum observed at 3500 cm^{-1} may be due to physically adsorbed water and O–H groups[9] on a solid surface. FTIR spectrum with varying concentrations of Dy, exhibiting identical absorption peaks as seen in **Figure 5**. Research suggests that altering Dy^{3+} content by doping does not influence the vibrational frequency of the nanopowders produced.

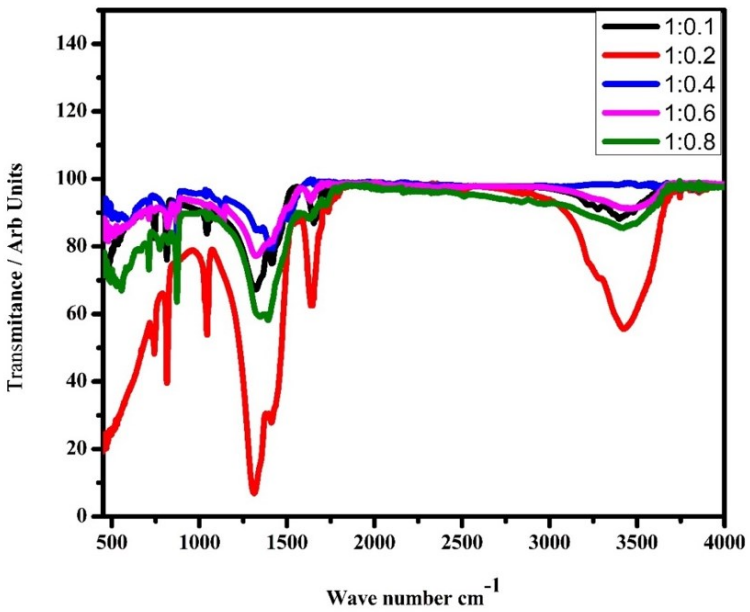

Figure 5 The FTIR spectra of $SrAl_2O_4$: Eu^{2+},Dy^{3+}prepared at varying Dy^{3+} concentration.

UV–Visible analysis

UV-visible spectra of $SrAl_2O_4$:Eu^{2+}, Dy^{3+} activated were measured within the 200-800 nm wavelength region. The generated $SrAl_2O_4$:Eu^{2+}, Dy^{3+}doped samples offer valuable data on the energy bandgap. A shift of absorption edges and bands to longer wavelengths was observed (**Figure 6**) (when molar ratios were increased from 0.1 to 0.8 mol %. The red shift of the absorption peaks demonstrates the growth of the nanocrystals [29]. It could be attributed as a result of the movement of charges across the valence band towards the conduction band of $SrAl_2O_4$:Eu^{2+}, Dy^{3+} nanoparticles. Optical energy bandgap (Eg) of the produced materials was calculated using Tauc's related equations[13].

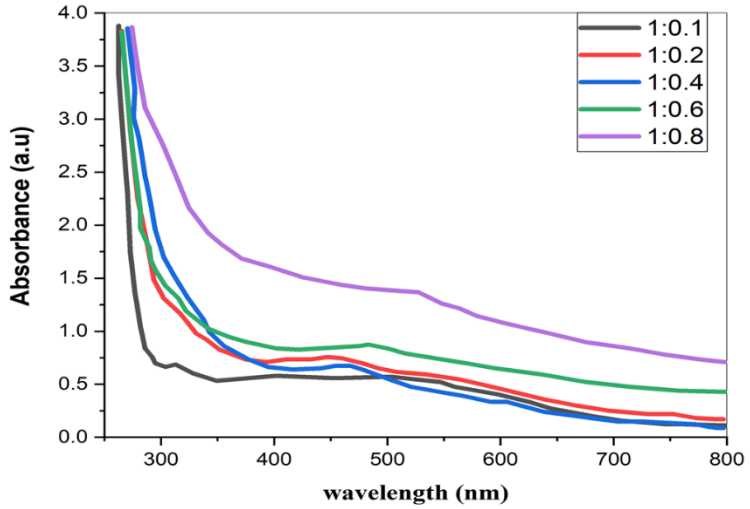

Figure 6 UV-Vis spectra showing absorbance versus wavelength

To determine the bandgap, we extrapolate the straight line section of the αhv against the hv graph to zero, with hv [30] as shown in **Figure 8**. The bandgap magnitude reduced from 6.5 to 5.5 eV when the amount of Dy^{3+} dopant raises from 0.1 to 0.8 mol % (**Table 1**). Prior studies have also documented a

reduction in the bandgap when doping $SrAl_2O_4:Eu^{2+}$ with Dy^{3+} [31]. The absorption edge shifts towards longer wavelengths as the concentration of Dy^{3+}ions in the strontium aluminate lattice increases. Doping generates impurities band intensities within strontium aluminate co-dopant contaminants in the $SrAl_2O_4:Eu^{2+}$ formation may result in a reduction in bandgap energy, causing the formation of novel interaction centers with lower emitting potential. With a rise in the quantity of Dy^{3+}, a greater number of electron traps are formed, Dysprosium (Dy) are added to modify the $SrAl_2O_4:Eu^{2}$, Dy^{3+}. As the same time, additional hole traps are created in the host material to maintain the charges balance (**Figure 7**). Increasing the overall of trapped electron and hole traps has a favorable effect on the optical properties of as-prepared material [3,30].

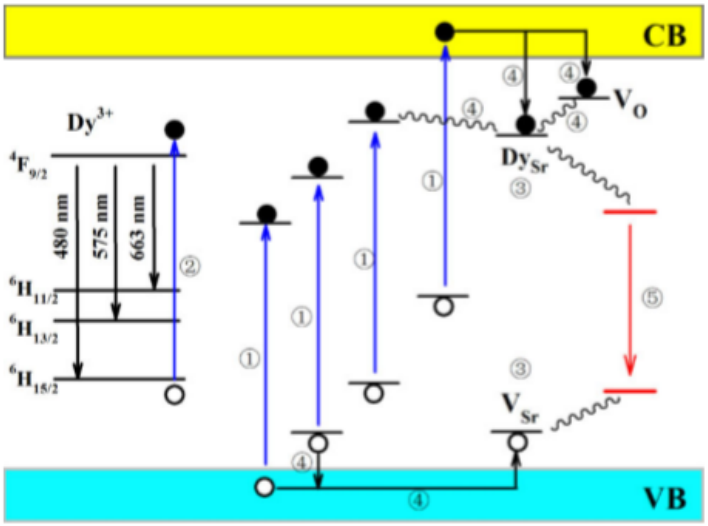

Figure 7 An analytical framework for interpreting the optical properties that vary with the concentration of dopants [32,33].

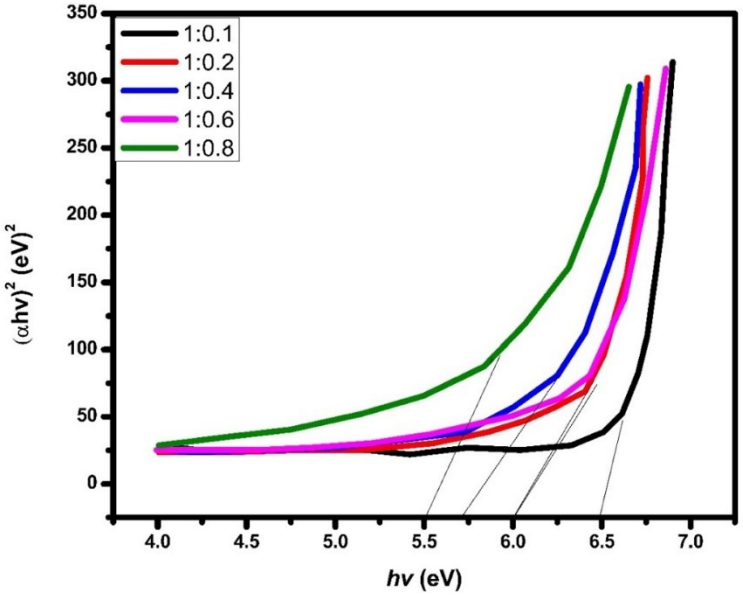

Figure 8 Tauc plot $(\alpha hv)^2$ against phonon energy.

Conclusions

The NPs of $SrAl_2O_4:Eu^{2+}$, Dy^{3+} were effectively synthesized using a solution combustion method, with different amounts of Dy^{3+}. The XRD tests showed the existence of nanocrystalline nanoparticles in a monoclinic phase. The crystallite sizes of the prepared $SrAl_2O_4:Eu^{2+}$, Dy^{3+} phosphor decreased as the concentration of Dy^{3+} calculated based on the Debye–Scherrer equation and W-H plot. The discrepancy in crystallite size obtained from the methods is due to the Williamson and Hall accounting for broadened produced by tensile strain factors. The UV-Vis analysis displayed the temperature-dependent properties of the synthesized $SrAl_2O_4:Eu^{2+}$, Dy^{3+}sample. Optical analysis showed that introducing Dy^{3+} into the $SrAl_2O_4:Eu^{2+}$, Dy^{3+} structure decreased the bandgap energy from 6.5 to 5.5 eV. The red shift seen in the bandgap was caused by the incorporation of Dy^{3+} ions into the host lattice, resulting in the creation of additional energy levels within the bandgap. As the Dy^{3+} concentration increased, the absorption edges (300 - 400 nm) showed a redshift. When the level of Dy^{3+} ions in the strontium aluminate lattice goes up, the absorption edge changes towards longer wavelengths. Doping generates impurities band intensities within strontium aluminate co-dopant contaminants in the $SrAl_2O_4:Eu^{2+}$, Dy^{3+} formation may result in a reduction in bandgap energy, causing the formation of novel interaction centers with lower-emitting potential. The Dy^{3+} concentration is essential for producing $SrAl_2O_4:Eu^{2+}$, Dy^{3+} nanoparticles with the best structural and optical properties. The $SrAl_2O_4:Eu^{2+}$, Dy^{3+}nanoparticles, prepared at 0.4 mol %, displayed desirable properties for making a glowing sign for occupational safety applications.

Acknowledgments

The authors thank Murang'a University of Technology, Pwani University, and Meneng'ai Geothermal Power Plant, Kenya for their help in performing the characterization of the prepared samples at their centers.

References

[1] AM Achari, V Perumalsamy, G Swat and A Khare. $SrAl_2O_4$: Eu^{2+}, Dy^{3+} long afterglow phosphor and its flexible film for optomechanical sensing application. *ACS Omega* 2023; **8**, 45483-94.

[2] J Bierwagen, T Delgado, G Jiranek, S Yoon, N Gartmann, B Walfort, M Pollnau and H Hagemann. Probing traps in the persistent phosphor $SrAl_2O_4$: Eu^{2+}, Dy^{3+}, B^{3+} - A wavelength, temperature and sample dependent thermoluminescence investigation. *J. Lumin.* 2020; **222**, 117113.

[3] PK Litoriya, S Kurmi and A Verma. Structural, optical, morphological and photoluminescence properties of $SrAl_2O_4$: Dy by using urea fuel combustion method. *Mater. Today Proc.* 2022; **66**, 2044-9.

[4] T Delgado, N Gartmann, B Walfort, F Lamattina, M Pollnau, A Rosspeintner, J Afshani, J Olchowka and H Hagemann. Fundamental loading-curve characteristics of the persistent phosphor $SrAl_2O_4$: Eu^{2+}, Dy^{3+}, B^{3+}: The effect of temperature and excitation density. *Adv. Photonics Res*. 2022; **3**, 2100179.

[5] H Xue, M Yang, J Sun and C Zhang. Study on the flux for SrAl2O4: Eu^{2+}, Dy^{3+} phosphor preparation used in fluorescent fiber. *Ceram. Int.* 2024; **50**, 1137-46.

[6] X Shen, S Tang, Q Hu and M Ge. Doping $SrAl_2O_4$: Eu^{2+}, Dy^{3+} and thermochromic materials for the generation of anticounterfeiting membrane. *ECS J. Solid State Sci. Tech.* 2020; **9**, 076001.

[7] Y Guo, Z Jiao, L Cao and S Li. The effect of trivalent ions on luminescent properties of $SrAl_2O_4$: Eu^{2+}, Dy^{3+} Phosphors. *J. Phys. Conf. Ser.* 2023; **2578**, 012009.

[8] X Duan, L Yi and S Huang. Structural and optical properties of size and morphology controllable nanoscale $SrAl_2O_4$: Eu^{2+}, Dy^{3+}. *Integr. Ferroelectr.* 2020; **210**, 74-82.

[9] S Fouzar, T Eftimov, I Kostova, A Benmounah and A Lakhssassi. Effects of temperature on the time responses of strontium aluminates. *Opt. Mater.* 2021; **122**, 111619.

[10] S Khursheed, GA Sheergojri and J Sharma. Phosphor polymer nanocomposite: $SrAl_2O_4$: Eu^{2+}, Dy^{3+} embedded PMMA for solid-state applications. *Mater. Today Proc.* 2020; **21**, 2096-104.

[11] P Gao, Q Liu, J Wu, J Jing, W Zhang, J Zhang, T Jiang, J Wang, Y Qi and Z Li. Enhanced fluorescence characteristics of $SrAl_2O_4$: Eu^{2+}, Dy^{3+} phosphor by co-doping Gd^{3+} and anti-counterfeiting applicatio. *Nanomater* 2023; **13**, 2034.

[12] S Kiprotich, B Dejene and M Onani. Effects of precursor pH on structural and optical properties of CdTe quantum dots by wet chemical route. *J. Mater. Sci. Mater. Electron.* 2018; **29**, 16101-10.

[13] Q Zhang, Y Xiong, Q Shi, Y Shi, M Niu, W Liu, T Wu, L Wang, Z Zhou and Q Liu, Effect of Ce^{3+} on the luminescence properties of $SrAl^2O^4$: Eu^{2+}, Dy^{3+} persistent phosphors for alternating current driven light-emitting diodes. *Russ. J. Inorg. Chem.* 2022; **67**, 1442-50.

[14] LHC Francisco, RP Moreira, MCFC Felinto, VC Teixeira, HF Brito and OL Malta. $SrAl_2O_4$: Eu^{2+}, Dy^{3+} persistent luminescent materials functionalized with the Eu^{3+} (TTA)-complex by microwave-assisted method. *J.Alloys Compd.* 2021; **882**, 160608.

[15] A Huang, Y Wu, Z Pan, B Wang and X Liang. Fabrication, characterization, and optimization of the composite long afterglow material $Sr_2MgSi_2O_7$: Eu^{2+}, Dy^{3+}@ $SrAl_2O_4$: Eu^{2+}, Dy^{3+}. *J. Sol-Gel Sci. Technol.* 2023; **105**, 500-10.

[16] R Lazau, R Ianos, C Pacurariu, DA Capraru, A Racu and V Cornea. Combustion synthesis of SrAl2O4: Eu2+, Dy3+ phosphorescent pigments for glow-in-the-dark safety markings. *Nanomater* 2023; **13**, 687.

[17] D Kshatri and A Khare. Optical properties of rare earth doped strontium aluminate (SAO) phosphors: A review. *Opt. Spectrosc.* 2014; **117**, 769-83.

[18] Z Ni, T Fan, S Bai, S Zhou, Y Lv, Y Ni and B Xu. Effect of the concentration of $SrAl_2O_4$: Eu^{2+} and Dy^{3+} (SAO) on characteristics and properties of environment-friendly long-persistent luminescence composites from polylactic acid and SAO. *Scanning* 2021; **2021**, 1-9.

[19] AH Wako, F Dejene and H Swart. Effect of Ga^{3+} and Gd^{3+} ions substitution on the structural and optical properties of Ce^{3+}-doped yttrium aluminium garnet phosphor nanopowders. *Luminescence* 2016; **31**, 1313-20.

[20] D Kshatri and A Khare. Characterization and optical properties of Dy^{3+} doped nanocrystalline $SrAl_2O_4$: Eu^{2+} phosphor. *J. Alloys Compd.* 2014; **588**, 488-95.

[21] R Tanaka, K Uematsu, M Sato and K Toda. Afterglow improvement of high concentration Dy^{3+} co-doped $SrAl_2O_4$: Eu^{2+} phosphor prepared by H_3BO_3 free synthesis using melt quenching method. *J. Ceram. Soc. Jpn.* 2021; **129**, 372-6.

[22] AH Wako, F Dejene and H Swart. Combustion synthesis, characterization and luminescence properties of barium aluminate phosphor. *J. Rare Earths* 2014; **32**, 806-11.

[23] E. Nurbaisyatul, H Azhan, N Ibrahim and S Saipuddin. Structural and superconducting properties of low-density Bi (Pb)-2223 superconductor: Effect of Eu_2O_3 nanoparticles addition. *Cryogenics* 2021; **119**, 103353.

[24] MRS Nasuha, H Azhan, L Hasnimulyati, WAW Razali and Y Norihan. Effect of Nd^{3+} ions on physical and optical properties of yttrium lead borotellurite glass system. *J. Non-Cryst. Solids* 2021; **551**, 120463.

[25] NNN Roslan, WAW Razali, AR Tamuri, H Azhan and Z Mohamed. Synthesis of green phosphor $SrAl_2O_4$: Eu^{2+}, Dy^{3+}: Rietveld refinement and optical properties. *Chalcogenide Lett.* 2022; **19**, 83-91.

[26] Y Zhu, Q Yu, L Zheng, Z Pang and M Ge. Luminous properties of recycling luminous materials $SrAl_2O_4$: Eu^{2+}, Dy^{3+} based on luminous polyester fabric. *Mater. Res. Express* 2020; **7**, 095309.

[27] N Takeuchi and K Kishine. Effect of addition of boron on the long afterglow property of $SrAl_2O_4$: Eu^{2+}, Dy^{3+} phosphor. *Mater. Trans.* 2021; **62**, 1039-45.

[28] P Gao, J Wang, J Wu, Q Xu, L Yang, Q Liu, Y Qi and Z Li. Preparation of SrAl2O4: Eu^{2+}, Dy^{3+} powder by combustion method and application in anticounterfeiting. *Coatings* 2023; **13**, 808.

[29] R Neema, M Saleem, P Sharma and M Mittal. Structure, optical bandgap and luminescence studies of $SrAl_2O_4$: Eu^{3+}, Dy^{3+} nanophosphor. *AIP Conf. Proc.* 2020; **2220**, 020159.

[30] R Neema, M Saleem, PK Sharma and M Mittal. Rare-earth Ion (Eu^{3+} and Dy^{3+}) substituted $SrAl_2O_4$ phosphor: A study of structural and luminescence properties. *AIP Conf. Proc.* 2021; **2369**, 020204.

[31] T Li, Q Liu, D Zhu, P Chen, Y Jing, J Wu, H Chen, D Hreniak, M Nikl and J Li. Fabrication and characterizations of Eu^{2+}-Dy^{3+} co-doped $SrAl_2O_4$ ceramics with persistent luminescence. *J. Am. Ceram. Soc.* 2023; **106**, 5877-86.

[32] KR Ashwini, HB Premkumar, BD Prasad, GP Darshan, H Nagabhushana, SC Sharma and SC Prashantha. Green emitting $SrAl_2O_4$: Tb^{3+} nano-powders for forensic, anti-counterfeiting and optoelectronic devices. *Inorg. Chem. Commun.* 2021; **130**, 108665.

[33] SK Sharma, J James, SK Gupta and S Hussain. UV-A, B, C emitting persistent luminescent materials. *Materials* 2023; **16**, 236.